Morphological investigation and magnetic properties of nickel zinc ferrite 1D nanostructures synthesized via thermal decomposition method

DATASET · OCTOBER 2013

5 AUTHORS, INCLUDING:

Said El-Sheikh
Central Metallurgical Research and De…
60 PUBLICATIONS **336** CITATIONS
SEE PROFILE

Mohamed M Rashad
Central Metallurgical Research and De…
133 PUBLICATIONS **1,558** CITATIONS
SEE PROFILE

Farid A. Harraz
Central Metallurgical Research and De…
69 PUBLICATIONS **936** CITATIONS
SEE PROFILE

J Nanopart Res (2013) 15:1967
DOI 10.1007/s11051-013-1967-9

RESEARCH PAPER

Morphological investigation and magnetic properties of nickel zinc ferrite 1D nanostructures synthesized via thermal decomposition method

Said M. El-Sheikh · Mohamed M. Rashad · Farid A. Harraz

Received: 12 November 2012 / Accepted: 22 August 2013 / Published online: 4 September 2013

Abstract Spinel nickel zinc ferrite nanowires were successfully prepared in mesoporous silica SBA-15 as a host matrix. The powder was annealed at a range of temperatures (500–900 °C) with heating rate 0.5 °C/min. The required $NiZnFe_2O_4$ phase was obtained at 700 °C. The specific surface area S_{BET} data revealed that the surface area of the mesoporous silica after annealing was decreased from 821 to 90 m^2/g which indicated that the spinal ferrite fills the channels of mesoporous materials. The one-dimensional spinel nanostructures were characterized by X-ray diffraction, infrared spectroscopy, vibrating sample magnetometer, and transmission electron microscopy before and after a selective removal of the silica template in aqueous solution of NaOH or HF. The presence of SBA-15 lowers the formation temperature of nickel zinc ferrite nanowires compared to the corresponding bulk material. The magnetic properties revealed a high saturation magnetization level ($\sim$43 emu/g) for the Ni–Zn nanowires at 900 °C.

Keywords Nickel zinc ferrite · Nanowires · Template synthesis · Thermal decomposition · Magnetic properties

S. M. El-Sheikh (✉) · M. M. Rashad · F. A. Harraz
Advanced Materials Technology Department, Central Metallurgical Research and Development Institute (CMRDI), P.O. Box 87, Helwan, Cairo 11421, Egypt
e-mail: selsheikh2001@gmail.com

Introduction

The magnetic nanowires represent an important family of magnetic nanostructures. For example, highly anisotropic magnetic nanowires possess ferromagnetic properties at room temperature even at diameters of 2 nm (Eliseeva et al. 2005). Nanowires possess unusual properties, e.g., quantum mechanical confinement effects, high surface to volume ratio, high anisotropy and they have the ability to connect the individual molecules (Ma et al. 2013; Kumar 2010d). Interestingly, one-dimensional (1D) magnetic nanowire has shown considerable promise as successful applications in giant magnetoresistance (GMR), biomedical applications, and magnetic sensors where minimal coercive force and high magnetization are necessary. However, order structure is essential for magnetic recording media such as the read head in present day computer, hard disks, and other magnetic storage devices where high coercivity and high magnetization are required to reduce the risk of data becoming corrupted when they are exposed to stray magnetic fields (Fert and Piraux 1999; Hessien et al. 2007; Han et al. 2002; El-Sheikh et al. 2010). Therefore, there is continued interest in simpler ways to fabricate and manipulate magnetic nanowires. The key synthetic methodologies to fabricate 1D magnetic nanowires include in plane growth via trench template-assisted technique (Kumar 2010b; Kumar et al. 2008b), electric field-induced growth (Kumar et al. 2008a; Kumar 2010b), template-assisted assembly,

direct self-assembly, laser-induced self-assembly, template-assisted electrodeposition (Kumar 2010a; Krishna and Kumar 2009), catalyzed high-temperature growth via the vapor–liquid–solid (VLS) mechanism (Morales and Lieber 1998; Ajayan 1999), metallization of DNA (Cu et al. 2005), solvothermal synthesis (Hu et al. 2008), and organometallic precursor decomposed in solution (Wang et al. 2003).

The physical characteristics of nanowires grown in this manner depend, in a controllable way, upon the size and physical properties. Nanowire arrays (anisotropic growth features) have been observed to form in the direction of electric field for DC electric field treatment case whereas ruptured isotropic growth features have been noticed for excimer laser case. For trench template-assisted technique, nanowires have grown along the length of trench template. Volume of material, growth features, flatness of the grain results, size, shape, separation of grains, and finally different extent of oxidation; these are the factors basically responsible for different magnetic behaviors shown in nanostructured magnetic materials (Kumar 2010c). For instant, preparation of nanocomposites based on spinel ferrites dispersed in silica is one of the research topics that recently received increasing attention (Xu et al. 2007). This is actually because ferrite nanoparticles usually have a strong tendency to aggregate, which makes it difficult to exploit their unique physical properties. Nanocomposites can effectively retain the nature of the nanocrystals by dispersing them in inorganic matrices because of the expected limited particle agglomeration and narrow grain size distribution (Kumar et al. 2009). Although much work has been devoted to the synthesis of metal nanowires in mesoporous templates, the preparation of Ni–Zn ferrite nanowires has been less explored. Yu et al. (2007) fabricate highly ordered $Ni_{0.5}Zn_{0.5}Fe_2O_4$ nanowire/tube arrays by the sol–gel method in the pores of anodic alumina membrane (AAM). Additionally, (Yang et al. 2010) synthesized $Ni_{0.23}Cu_{0.11}Zn_{0.66}Fe_2O_4$ nanowire arrays by a simple ethanol-nitrate method using AAM templates. To date there are challenges to control the size and morphology, crystallinity and unidirectional growth of nanowires. To the best of our knowledge, no study has been reported for the preparation of 1D nickel zinc ferrite nanowires using as-synthesized mesoporous silica SBA-15 template. Mesoporous silica such as SBA-15 is commonly used as a host matrix for fabricating nanowires, due to its homogenous and well-ordered channel structures of pores (5–7 nm) with high surface area ($\approx$900 m^2 g^{-1}) and thermal stability (Eliseeva et al. 2005). Furthermore, the magnetic characteristics of such nanowires still need to be investigated for their further possible use in magnetic storage media.

The aim of the present work is to fabricate nickel zinc ferrite nanowires with controlled size and shape by employing a template-assisted technique; mesoporous silica SBA-15 template is utilized in this study. Different annealing temperatures ranging from 500 to 900 °C with heating rate 0.5 °C were used to identify the best formation temperature of nanowires. The magnetic properties of as-synthesized nanostructures were also correlated with the controlling reaction parameters and annealing temperatures.

Experimental

Hexagonally ordered SBA-15 was synthesized, following the procedure described in Ref. (Zhao et al. 1998), in acidic media using poly(ethylene glycol)–poly(propylene glycol)–poly(ethylene glycol) triblock copolymer, $EO_{20}PO_{70}EO_{20}$ (Pluronic 123) as a templating agent. In a typical preparation method, 8 g Pluronic 123 was dissolved in 60 ml water and 240 ml 2N HCl solution at 35 °C. After addition of 18.2 ml tetraethyl orthosilicate (TEOS), the reaction mixture was stirred at 35 °C for 24 h and then at 80 °C for 48 h. The final solid product was separated by filtration, washed with water, and dried in air at room temperature. The resulting material was evacuated at 350 °C for 2 h and left under vacuum for 24 h before using.

The $NiZnFe_2O_4$ nanostructures were synthesized as follows: the iron, zinc, and nickel precursors 13.80 g $Fe(NO_3)_3{\cdot}9H_2O$, 5.03 g $Zn(NO_3)_2{\cdot}6H_2O$, and 5.03 g $Ni(NO_3)_2{\cdot}6H_2O$ were first dissolved in a 10 ml deionized water with 2:0.5:0.5 molar ratio of Fe/Zn/Ni. The volume of solution was identical to the pore volume of SBA-15 (1.05 cm^3/g) as determined by analysis of surface area and pore volume of the sample. 1.05 ml of previous solution was added dropwise to a flask containing stirred solution of 1 g SBA-15 dispersed in (20 ml) of methanol. Then, the flask was closed and the resulting mixture was left stirring overnight for a complete impregnation process (Fukuoka et al. 2006). The flask was then opened with

continuous stirring the mixture until a complete removal of the solvent. The filled material was then dried in air in an oven at 100 °C for 2 h.

The calcination process of the as-prepared samples was performed separately in a tube furnace equipped with a tubular quartz reactor at 500, 700, and 900 °C for 5 h with heating rate 0.5 °C/min in air. About 3 g of each sample was put in a crucible and the designated calcination temperatures were left for 5 h after the temperature raising from room temperature with rate of 0.5 °C/min. The produced samples are denoted 500-B (before removal of template), 700-B, and 900-B, respectively. For the samples treated with citric acid, they were denoted 500-B-cit, 700-B-cit, and 900-B-cit, respectively. Then, nickel zinc ferrite nanowires were released from the template by dissolving the as-prepared nanocomposites (500 and 700 °C) in 2.0 M NaOH, while the samples calcined at 900 °C were dissolved in 10 % HF for 8 h and collected by repeating centrifugation and washing with water and ethanol followed by drying at 100 °C for 2 h. In order to observe the nanostructured materials formed inside SBA-15 channels, a hot 2 M aqueous NaOH (500–700 °C) and 10 % HF (900 °C) solution were used to dissolve the silica template. The samples are denoted after washing and removal of template, 500-w, 700-w, 900-w, 500-w-cit, and 700-w-cit, respectively.

Phase identification, purity, relative crystallinity, and crystallite size of the produced powder are preformed at room temperature by X-ray diffraction (XRD, Bruker axs D8, Germany) with Cu Kα ($\lambda = 1.5406$ Å) radiation and secondary monochromator in the range 2θ from 20° to 80°. Relative crystallinity is estimated from the area under the most intense peak plane of XRD patterns. Crystallite size is automatically calculated from XRD data. Specific surface area (S_{BET}), pore volume, and pore size distribution of the powder are determined by BET surface area analyzer (Nova 2000 series, Quantachrome Instruments, UK). The microstructures of the formed samples are investigated using transmission electron microscopy (TEM, JEOL-JEM-1230, Japan). Infrared absorption spectroscopy (IR) was performed by JASCO 3600 spectrophotometer. The magnetic properties of the produced ferrites powders were characterized using a vibrating sample magnetometer (VSM; lakeshore 7400, USA) at room temperature in a maximum applied field of 32 kOe. From the obtained hysteresis loops, the saturation magnetization (M_s), remanence magnetization (M_r), and coercivity (H_c) were determined.

Results and discussion

Characterization of as-formed nanostructures

X-ray diffraction analysis (XRD)

The XRD patterns of nickel zinc ferrite nanostructures obtained before and after removal of the silica templates in 2 M NaOH and annealed at different temperatures (500 and 700 °C) are shown in Fig. 1a. Below 700 °C (before removal of silica), XRD patterns exhibit a diffraction hump around $2\theta = 14°–30°$, which belongs to the amorphous silica walls of SBA-15 for samples 500-B (data not shown) and 500-0.5-B-cit. Whereas from 700 °C the diffraction pattern can be indexed to the spinel nickel zinc ferrite phase for the samples 700-0.5-B and 700-0.5-B-cit, respectively. On the other hand, upon removal of template in 2NaOH), it can be seen that a weak crystalline phase is formed at low temperature of 500 °C for sample 500-0.5 W. Peaks at 2θ of 30.07°, 35.42°, 37.05°, 43.09°, 63.42°, 56.94°, 62.56°, 71.02°, and 74.02° related to XRD diffraction planes (2 2 0), (3 1 1), (2 2 2), (4 0 0), (4 2 2), (5 1 1), (4 4 0), (6 2 0), and (5 3 3) were clearly presented in the sample (700-0.5 W). These peaks confirmed that cubic spinel nickel–zinc ferrite (JCPDS# 08-0234) was formed in a well crystalline form. It can be noticed that, the XRD patterns of the formed precursor in the presence of citric acid as a complexing agent and as a fuel annealed at 500 and 700 °C, have a similar behavior to the samples prepared without the addition of citric acid.

The resulting XRD patterns of the Ni–Zn ferrite samples annealed at 800 and 900 °C are shown in Fig. 1c. However, at 800 °C reflection characteristics appeared of an unwanted phase (α-Fe_2O_3 (Montemayor et al. 2005) as a minor component marked as circular in the figure beside spinel nickel zinc ferrite phase. The similar trend was observed for the previous published report by Montemayor et al. in which α-Fe_2O_3 was matched with the $CoFe_2O_4$ for the sample annealed at 800 °C. As one can observe, a further increase in annealing temperature to 900 °C led to

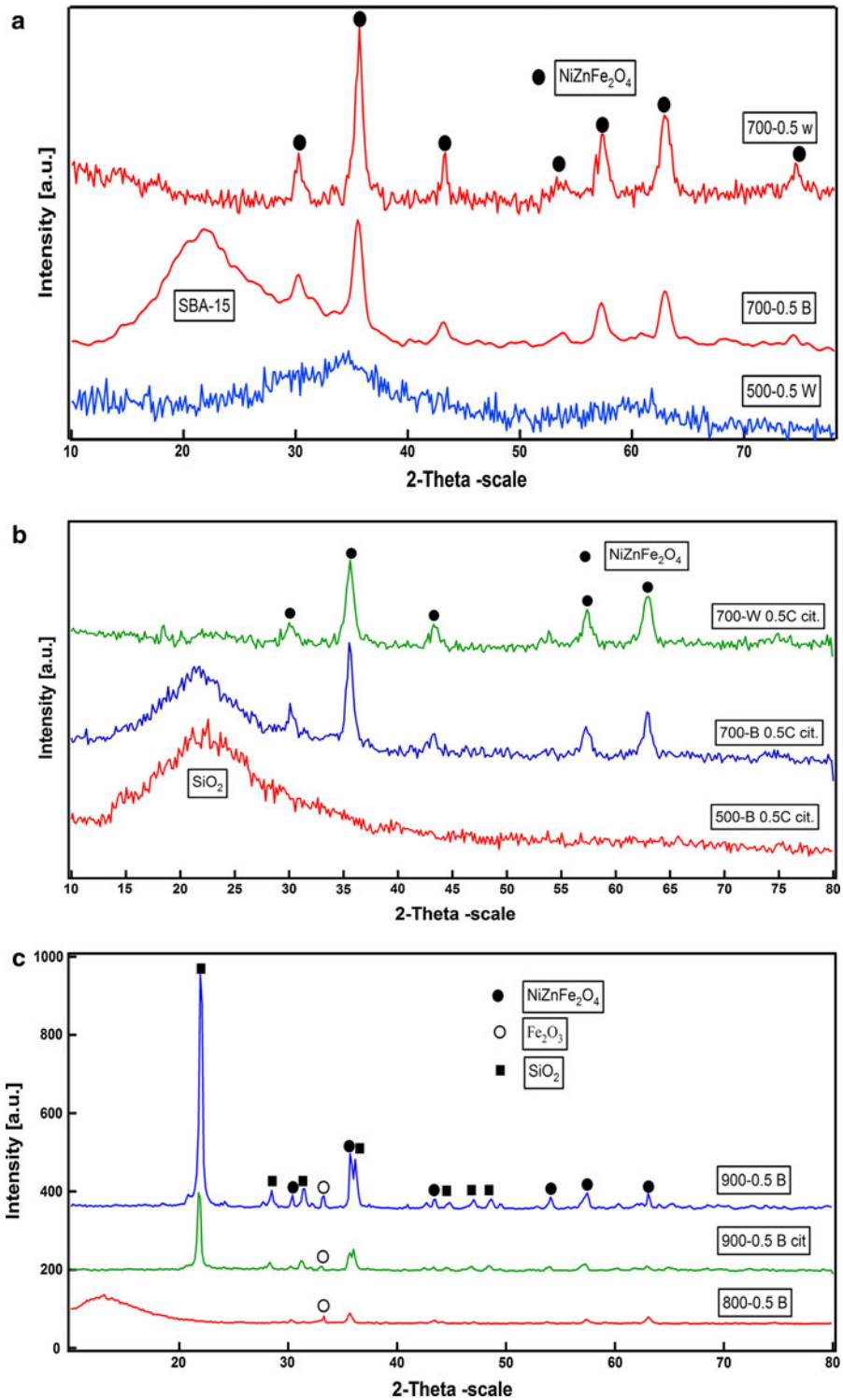

Fig. 1 XRD patterns of nickel zinc ferrite nanostructures obtained at different annealing temperatures of 500 and 700 before and after removal of silica template: **a** without citric acid and **b** with citric acid. **c** XRD patterns of released nickel zinc ferrite nanostructure annealed at 800 and 900 °C

increasing the crystallization rate of spinel Ni−Zn ferrite, simultaneously with the appearance of α-Fe_2O_3 (hematite) phase (JCPDS# 89-0598) and the silica template was crystallized to cristobalite phase. The formation of such iron oxide phase in 800–900 °C samples may be related to the different mobilities of

iron, nickel, and zinc ions under the present experimental conditions. This may result in a faster diffusion of iron ions to the mesoporous silica outer surface, which in turn may lead to the formation of iron oxide particles outside the porous structure. This means that the presence of silica-based template not only confined the wire formation but also lowered the formation temperature of Ni–Zn ferrite phase.

The XRD results indicate consequently that a complete phase transformation to spinel phase of Ni–Zn Fe_2O_4 inside SBA-15 nanopores is achieved above 700 °C with the observation of increasing the degree of crystallinity with annealing temperature. Furthermore, the lattice parameters, unit cell volume, and crystallite size determined from the most intense diffraction peaks (311) for the different prepared ferrite compositions, applying Debye–Scherrer equation, showed that the crystallite size was increased from 12 to 37 nm with increasing the annealing temperature from 700 to 900 °C as shown in Table 1.

Surface area

Figure 2 shows the isotherms of SBA-15 and NiZnFe$_2$O$_4$ phase treated at 700 °C with and without citric acid. The BET surface area, pore volume, and average pore diameter of pristine SBA-15 are 821 m^2/g, 1.05 cm^3/g, and 5–7 nm, respectively, as listed in Table 2. In contrast, these data of the samples containing nickel zinc ferrite sharply decrease. For the sample treated at 700 °C without and with citric acid, BET surface area is 90 and 84 m^2/g, respectively. This is due to the slightly high loading of $NiZnFe_2O_4$ inside the pores of SBA-15.

Fourier transform infrared spectroscopy (FT-IR)

Figure 3a, b shows FT-IR spectra recorded in 400–4,000 cm^{-1} range for as-synthesized NiZnFe$_2$O$_4$/SBA-15 nanocomposite prepared with different temperatures from 500 to 900 °C in the presence of citric acid and without. Four intensive absorption bands are observed at 1,230–1,220, 1,094–1,084, 808–803, and 466 cm^{-1} which can be assigned to asymmetric and symmetric stretching vibration of Si–O–Si framework of SAB-15 template. The broad absorption bands detected at 3,441–3,427 and 1,639–1,630 cm^{-1} and the weak band appeared at 981–966 cm^{-1} are related to Si–OH stretching and bending vibration, respectively. An OH stretching vibration due to physisorbed water near 3,441 cm^{-1} is observed with an OH deformation vibration near 1,639 cm^{-1} due to potentially surface hydroxyls (Shen et al. 2004; Ma et al. 2003). The intensity of OH peak decreased with increasing temperature. This means that a new metal ferrite silicon oxide bond is formed in expense of Si–OH. The absorption band observed at 2,925–2,929 cm^{-1}, may be related to the presence of aliphatic CH group generated from citric acid decomposition. Traces of adsorbed or atmospheric CO_2 were also evidenced by the very light band around 2,355 cm^{-1}.

Table 1 Average crystallite size from XRD, lattice parameters, unit cell volume, and non-crystalline volume percentage of for Ni–Zn ferrite nanostructures grown at different temperatures by the assistance of mesoporous silica template

Sample no.	Temperature (°C)	Average crystallite size from XRD (nm)	d (Å)	Cubic $a = b = c$	Unit cell volume (Å^3)	Non-crystalline volume percentage (%)
500-B	500	Amorphous				
500-w	500	10.7	2.5114	8.329	577.86	13
500-B-cit	500	Amorphous				
700-B	700	13.8	2.5180	8.351	582.41	37
700-w	700	13.9	2.5133	8.337	579.17	32
700-B-cit	700	15.9	2.5169	8.346	581.53	35
700-w-cit	700	14.8	2.5133	8.335	579.23	30
800	800	35	2.5160	8.344	581.09	33
900-B	900	37.1	2.5125	8.332	578.62	100
900-B-cit	900	32.7	2.5128	8.333	578.81	80

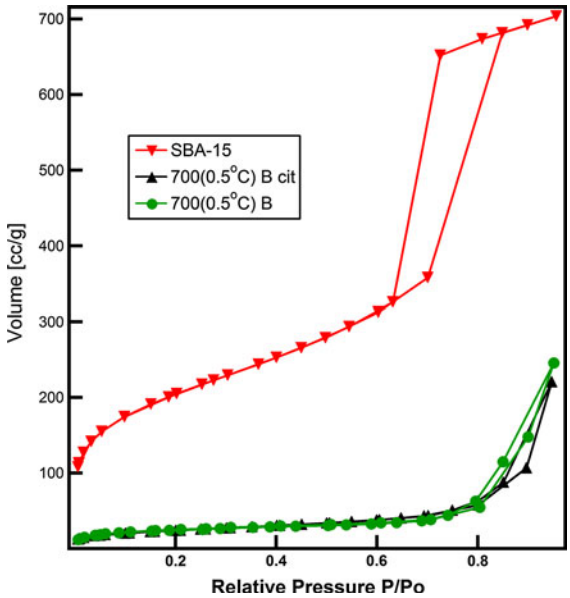

Fig. 2 Nitrogen adsorption–desorption isotherm of SBA-15 and NiZn ferrite/SBA-15 nanocomposites synthesized at 700 °C in the presence of citric acid and without

A broad band of the spinel ferrites, corresponding to the metal-oxide (M–O (M = Fe, Ni, Zn) bands in ($NiZnFe_2O_4$) intrinsic stretching vibrations at the tetrahedral site, could be seen at around 500–700 cm^{-1} and centered at 603–619 cm^{-1} for the samples synthesized at the above stated temperatures (M-Bahout et al. 2005). On the other hand, the high frequency band found at 603–619 cm^{-1} is attributed to the tetrahedral complexes (Fe^{3+}–O^{2-}) and variation in the band position is due to the difference in the (Fe^{3+}–O^{2-}) distance for octahedral and tetrahedral complex (Shen et al. 2004). The presence of absorption band 800 cm^{-1} is evidence to the formation of Fe–Ni–Zn alloy in the Ni–Zn ferrite (M-Bahout et al. 2005; Wu et al. 2004; Kryszewski and Jeszka 1998). The lower absorption bands assigned to the octahedral-metal stretching are usually observed in the range 450–385 cm^{-1} (M-Bahout et al. 2005). The spinel structure which consists of eight formula units, eight (MFe_2O_4), forms a unit cell of the spinel lattice. The metal ions (M) are either surrounded by four oxygen ions, tetrahedral sites, or six oxygen ions, octahedral sites. In this study, the $NiZnFe_2O_4$, the Zn^{2+} ions sited on the tetrahedral sites, whereas the Ni^{2+} ions on the octahedral sites, and the remaining were filled by the 16 Fe^{3+} ions.

Figure 3c represents the FT-IR spectra of NiZ-nFe_2O_4 after release from silica template by NaOH. Consequently, the bands detected at 603–619 cm^{-1} were attributed to the tetrahedral Zn^{2+} vibrations, and the Fe^{3+} vibrations at the octahedral site as shown in Fig. 3c (M-Bahout et al. 2005). The band at 425 cm^{-1} is likely due to the transferred octahedral Ni^{2+} ions as the temperature increased from 500 to 700 °C. By increasing the temperature, one can observe a shift in band position to a higher wave number with increasing peaks sharpness, which is likely owing to the onset of crystallization (Liu et al. 2005).

Figure 3a–c shows that, in general the intensities of absorption bands are strong in case of citric acid. This proves that the citric acid facilitates the growth of ferrite inside SBA-15 compared to the case without citric acid. This is in a good agreement with surface area measurements obtained in Fig. 2 and Table 2.

Transmission electron microscopy (TEM)

The removal of silica template was performed by treating the as-formed nanocomposite in 2 M NaOH solution for samples prepared at a temperature <900 °C and in 10 % HF solution for samples prepared at 900 °C in order to release the NiZn ferrite initially formed inside silica nanotemplate. TEM images of the silica free samples calcined at 700 and 900 °C were taken and shown in Fig. 4. The image of ferrite sample calcined at 700 °C is shown in Fig. 4a.

Table 2 Surface area, pore volume, pore diameter, and some important FT-IR absorption bands for SBA-15, 700-B, and 700-B-Cit, respectively

Sample no.	SA (m^2/g)	Average pore volume (CC/g)	Average pore radius (nm)	Important FT-IR absorption bands
SBA-15	821	1.051	4.64	981–966 cm^{-1} are related to Si–OH
700-B	90	0.408	6.62	603–619 cm^{-1}, tetrahedral Zn^{2+} vibrations, and the Fe^{3+} vibrations 425 cm^{-1}, transferred octahedral Ni^{2+} ions
700-B-Cit	84	0.351	4.56	

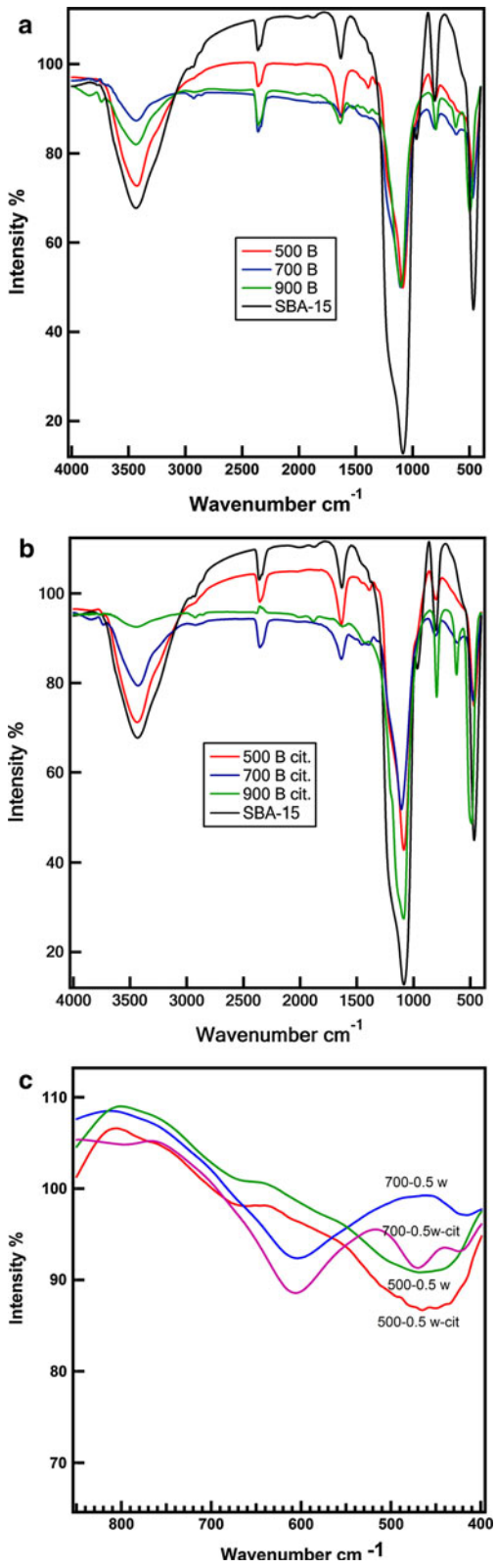

◀ **Fig. 3** FT-IR spectra of **a** nickel zinc ferrite/SBA-15 nanocomposite synthesized at different annealing temperatures without citric acid, **b** with citric acid, and **c** low wavelength of samples synthesized at 500 and 700 °C in the presence of citric acid and without after removal of silica

The diameter of the produced nanowires in the broadest region is ~8–10 nm, which is wider than the pore diameter of SBA-15 template (5–7 nm) as depicted in FFT inset of Fig. 4a. This may be due to the presence of micropores on silica walls of SBA-15 channels, which increased in diameter with increasing the calcination temperature (Ueno et al. 2005). During the annealing process, decomposition of the precursors extended from the mesoporous channels to microporous and led to the formation of 1D-nickel zinc ferrite. This means that our approach proves the formation of ordered nanowires for samples treated at 700 °C or above. This observation actually points out that the impregnation of SBA-15 matrix by nickel, zinc, and iron precursors followed by decomposition procedure at high temperatures has no significant effect on the pore structure of the host silica template.

With increasing calcination temperature to 700 °C, the length of spinel nickel zinc ferrite nanowires extended to reach about 14–15 μm in length image 4a. The 1D long nanowires of spinel nickel zinc ferrite grown and fill the nanochannels uniformly and the nanowires are apparently grown by further heating from 500 to 700 °C. This may be attributed to the small nanoparticles aggregate and the grain growing slowly reaching the compact at 700 °C to form long nanowires with a careful control of the reaction condition.

As shown earlier, the diameter of the nanowires and rods of as-synthesized nickel zinc ferrite and iron oxide (Fig. 4b–d) at 900 °C are larger than the pore diameter of the template which was probably due to the existence of micropores on the amorphous silica walls. These micropores led to the formation of channeled nickel zinc ferrite nanowires at a very high annealing temperature. Nickel, zinc, and iron precursors not only filled the mesopores but also are accessible into the micropores. With increasing annealing temperature, the diameter of these micropores increased and the distribution of micropore size become wider (Eliseeva et al. 2005). Thus, the decomposition of the precursor extended from the mesopores channel to the micropores during the calcination process. Hence, the highly crystalline

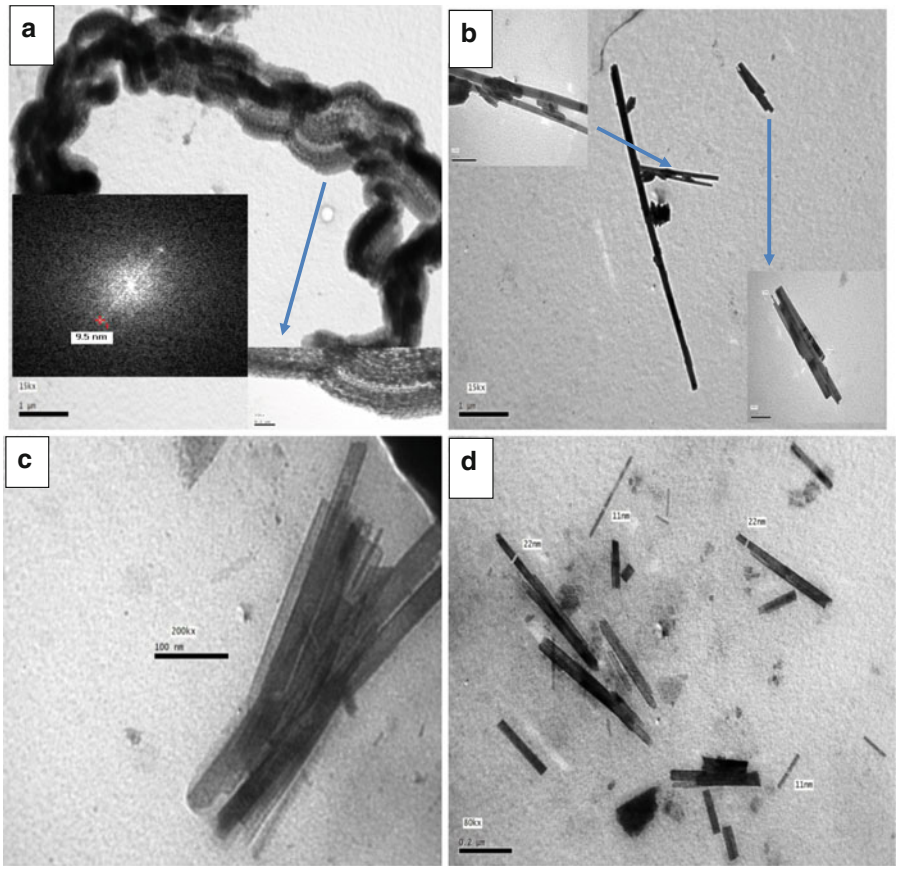

Fig. 4 TEM images for free nickel zinc ferrite nanostructures synthesized using silica-based template and annealed at **a** 700 °C, **b**–**d** magnified images synthesized at annealed at 900 °C

nickel zinc ferrite and iron oxide formed at 900 °C led to a diameter of the nanowires being larger than the pore diameter of the template. A two kinds of rods are formed as seen in Fig. 4c, d, the first is small one around diameter 11–12 nm and another one is around 25–30 nm. This may be related to the effect of temperature at 900 °C, at which a grain growth of nickel zinc ferrite and iron oxide inside the host matrix may take place followed by getting outside from the host matrix.

Magnetic properties

The magnetization of the produced Ni–Zn ferrite nanowires was measured at room temperature under an applied field of 15 kOe and the corresponding hysteresis loops were consequently obtained. Plot of magnetization (M) as a function of applied field (H) at different annealing temperatures from 500 to 900 °C is shown in Fig. 5 and the corresponding magnetic parameters are listed in Table 3. The results obtained indicate that the increase in the temperature led to increase the saturation magnetization (M_s). The saturation magnetization increased from 0.20 to 42.49 emu/g in the absence of citric acid whereas it increased from 4.49 to 41.26 emu/g in the presence of citric acid with increasing the annealing temperature from 500 to 900 °C. The values are smaller than the bulk value of Ni–Zn ferrites (65–115 emu/g) (Rashad et al. 2009). This reduction is due to the surface effect with decreasing particle size. M_s decreased with decreasing crystallite size for mono-domain particles due to the surface spin canting and thermal fluctuation (Sivakumar et al. 2012). Combined with XRD and TEM results, we suggest that well crystallinity of the samples and more formation of magnetic phase due to the higher temperature aroused the significant increase of M_s. The weak magnetism of the nanowires prepared

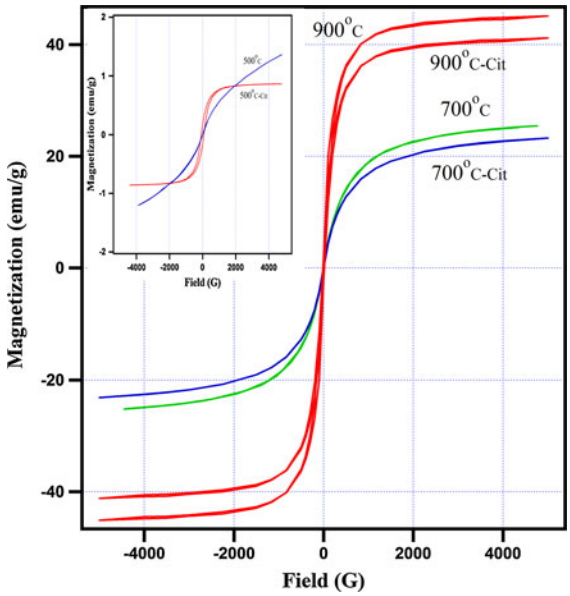

Fig. 5 Magnetic hysteresis behavior of nickel zinc ferrite nanowires produced by the template synthesis route and annealed at different temperatures between 500 and 900 °C using citric acid and without

at 500 °C was mainly due to the partial crystallization occurs in the samples treated at these temperatures. The large magnetization obtained at annealing temperatures 900 °C can be attributed to the increase of the crystallization rate (Zhang et al. 2009) as explained earlier in XRD results of Figs. 1 and 2.

The observed H_c is slightly increased from 4.72 to 15.74 Oe with increasing annealing temperature from 700 to 900 °C, whereas it increased from 3.82 to 13.69 Oe in the presence of citric acid. The increase of H_c with annealing temperature is likely related to the particle size varying with the temperatures. The nanowires are initially composed of nanoparticles. Upon the annealing temperature increases, the particle size in the nanowires is increased with temperature and leads to a change of the magnetic properties of the nanowires. The H_c is in direct proportion to the volume single-domain grains. Therefore, H_c becomes gradually larger as the single-domain particle size increases (Sivakumar et al. 2012). When the grain size reaches to a critical diameter of 40 nm (below which the particle is of a single-domain grain), the coercivity starts to increase. In particular, in real systems, the domain wall (DW) can be trapped by edge roughness, grain boundaries, and other pinning sites. Such pinning effects strongly influence the potential landscape for the DW and consequently its dynamics. In general, domain wall motions (DWM) in nanowires depend mainly on the domain wall velocity by spin waves (SWs), the SW dispersion and the depinning fields for pinned domain wall. On the other hand, the magnetization dynamics obtained are due to a spin polarized current and propagating SWs in magnetic nanowire. SWs are one of the basic perturbations in a magnetic system and these are the lowest collective excitations in magnetic lattices with continuous symmetry. The physical origin of the SW-induced DWM strongly depends on the propagating SW frequency. At certain SW frequencies, transverse domain wall oscillations lead to transverse wall displacement by the SWs, while at other frequencies, large reflection and effective momentum transfer are main drivers of the SW-induced DWM (Von 2011). Furthermore, highly deformed Neel type DW, as well as toroidal DW has been found in the wires with moderate aspect ratio due to the influence of the demagnetization field near the wire ends (Usov et al. 2007). Moreover, for the imperfect wires, it was anticipated that the strong influence of transverse anisotropic together with damping parameters will impact greatly the global wall dynamics (Thiaville et al. 2002). On the other hand, it is shown that the width of both types of DWs in the magnetic nanowires is in the ordered of the wires

Table 3 Magnetic properties, measured at room temperature, for Ni–Zn Ferrite nanostructures grown at different temperatures by the assistance of mesoporous silica template

Temperature (°C)	Magnetic properties					
	Without citric acid			With citric acid		
	M_s (emu/g)	M_r (emu/g)	H_c (Oe)	M_s (emu/g)	M_r (emu/g)	H_c (Oe)
500	0.17	0.009	21.74	4.32	0.008	5.95
700	25.32	0.23	4.73	23.82	0.17	3.82
900	42.49	1.89	15.74	41.26	1.84	13.69

diameters which lead to average mobility of vortex DW (Usov et al. 2007). This means a direct relation between the coercivity and DWMs. Additionally, nanowires have longitudinal magnetization due to the wall is charged from "head to head" (Thiaville et al. 2002). So, a key problem in the understanding the magnetism of nanowires is the diameters dependence of coercivity (Zeng et al. 2002; Pal et al. 2011). The coercivity is decreased or increased depending on the diameter and aspect ratio of the nanowires. Ferromagnetic nanowires with diameters in the range of domain wall width or smaller ($\leq$40 nm) are expected to behave as single-domain particles while particles larger than 40 nm are divided into domains and domain wall. The coercivity of the ferrite increases with increasing diameter and reaches a maximum values with diameter of critical single domain ($\sim$40 nm). Particles larger than critical single domains result in reduced coercivity with increasing size. This is because the domain wall displacement in the magnetization process is the multi-domain grains. Thus, the coercivity decreases with the growing of multi-domain grain.

Meanwhile, decreased in non-crystalline volume percentage calculated from XRD (Table 1) and pore size distribution calculated from BJH method (Table 2) led to decrease the saturation magnetization (M_s) and net coercivity. On the other hand, effective functional groups appeared in FT-IR at 603–619 cm^{-1}, related to tetrahedral Zn^{2+} and octahedral Fe^{3+} vibrations at 425 cm^{-1} related to transferred octahedral Ni^{2+} ions are the main respective relative effects in determining the magnetization and net coercive.

Conclusions

$NiZnFe_2O_4$ nanowire arrays were synthesized via thermal decomposition method using SBA-15 templates. The silica walls of SBA-15 behave as barrier for confined formation nanowires in addition to help lowering the wire formation temperature compared to the bulk materials. The nickel zinc ferrite nanowire arrays were uniformly distributed and well aligned. However, addition of citric acid was insignificant effect of the microstructure and magnetic properties of the formed ferrite powders. The specific surface area S_{BET} of the mesoporous silica after annealing was decreased from 821 to 90 m^2/g which indicated that the spinal ferrite fills the channels of mesoporous materials. FT-IR spectrum indicated that Ni–Zn ferrite powders have cubic spinel structure. High saturation magnetization 42.49 emu/g was achieved with increasing the annealing temperature to 900 °C. The present approach could be beneficial for fabrication of various ferrites and magnetic nanowires which are expected to be potential candidates for several current and future-related technologies.

References

Ajayan PM (1999) Nanotubes from carbon. Chem Rev 99:1787–1799

Cu Q, Cheng C, Haynie DT (2005) Cobalt metallization of DNA: toward magnetic nanowires. Nanotechnology 16(8):1358–1363

Eliseeva AA, Gorozhankina DF, Zaitseva DD, Lukashina AV, Knotkoa AV, Tretyakova Y-D, Gornert P (2005) Preparation of strontium hexaferrite nanowires in the mesoporous silica matrix (MCM-41). J Magn Magn Mater 290–291: 106–109

El-Sheikh SM, Harraz FA, Hessien MM (2010) Magnetic behavior of cobalt ferrite nanowires prepared by template-assisted technique. Mater Chem Phys 123:254–259

Fert A, Piraux L (1999) Magnetic nanowires. J Magn Magn Mater 200:338–358

Fukuoka A, Sakamoto Y, Higuchi T, Shimomura N, Ichikawa M (2006) Synthesis and electronic property of platinum nanowire and nanoparticle in mesoporous silica template. J Porous Mater 13:231–235

Han GC, Zong BY, Wu YH (2002) Magnetic properties of magnetic nano-wire arrays. IEEE Trans Magn 38(5):2562–2564

Hessien MM, Radwan M, Rashad MM (2007) Enhancement of magnetic properties for the barium hexaferrite prepared through ceramic route. J Anal Appl Pyrol 78:282–287

Hu MJ, Lin B, Yu SH (2008) Magnetic field-induced solvothermal synthesis of one-dimensional assemblies of Ni–Co alloy microstructures. Nano Res 1:303–313

Krishna MG, Kumar P (2009) Non-lithographic techniques for nanostructuring of thin films and bulk surfaces. In: Ahmed W, Jackson Mark J (eds) Emerging nanotechnologies for manufacturing. Elsevier Inc., Oxford, pp 93–130. ISBN 978-0-8155-1583-8

Kryszewski M, Jeszka JK (1998) Nanostructured conducting polymer composites super paramagnetic particles in conducting polymers. Synth Met 94:99–104

Kumar P (2010a) Directed self-assembly: expectations and achievements. Nanoscale Res Lett 5:1367–1376

Kumar P (2010b) Electric field and excimer laser nanostructuring of Ni and Si thin films. Adv Sci Lett 3:62–66

Kumar P (2010c) Magnetic behavior of surface nanostructured 50-nm nickel thin films. Nanoscale Res Lett 5:1596–1602

Kumar P (2010d) Trench-template fabrication of indium and silicon nanowires prepared by thermal evaporation process. J Nanoparticle Res 12:2473–2480

Kumar P, Krishna MG, Bhatnagar AK, Bhattacharya AK (2008a) Template-assisted fabrication of nanowires. Int J Nanomanuf 2:477–495

Kumar P, Krishna MG, Bhattacharya AK (2008b) Electric field induced nanostructuring of metallic thin films. Int J Nanosci 7:255–261

Kumar P, Krishna MG, Bhattacharya AK (2009) Effect of microstructural evolution on magnetic properties of Ni thin films. Bull Mater Sci 32:263–270

Liu XM, Fu SY, Xiao HM, Huang CJ (2005) Synthesis of nanocrystalline spinel $CoFe_2O_4$ via a polymer-pyrolysis route. Phys B 370:14–21

Ma M, Zhang Y, Yu W, Shen HY, Zhang HQ, Gu N (2003) Preparation and characterization of magnetite nanoparticles coated by amino silane. Colloids Surf A 212:219–226

Ma L-C, Zhang J-M, Xu KW (2013) Magnetic and electronic properties of Fe/Cu multilayered nanowires: a first-principles investigation. Physica E50:1–5

M-Bahout M, Bertrand S, Peoa O (2005) Synthesis and characterization of $Zn_{1-x}Ni_xFe_2O_4$ spinels prepared by a citrate precursor. J Solid State Chem 178:1080–1086

Montemayor SM, Garcı′a-Cerda LA, Torres-Lubia′n JR (2005) Preparation and characterization of cobalt ferrite by the polymerized complex method. Mater Lett 59:1056–1060

Morales AM, Lieber CM (1998) A laser ablation method for the synthesis of crystalline semiconductor nanowires. Science 279:208–211

Pal S, Saha S, Polley D, Barman A (2011) Magnetization reversal dynamics in Co nanowires with competing magnetic anisotropies. Solid State Commun 151:1994–1998

Rashad MM, Elsayed EM, Moharam MM, Abou-Shahba RM, Saba AE (2009) Structure and magnetic properties of $Ni_xZn_{1-x}Fe_2O_4$ nanoparticles prepared through co-precipitation method. J Alloys Compd 486:759–767

Shen XC, Fang XZ, Zhou YH, Liang H (2004) Synthesis and characterization of 3-aminopropyltriethoxysilane-modified super paramagnetic magnetite nanoparticles. Chem Lett 33:1468–1689

Sivakumar P, Ramesh R, Ramanand A, Ponnusamy S, Uthamizhchelvan C (2012) Preparation and properties of $NiFe_2O_4$ nanowires. Mater Lett 66:314–317

Thiaville A, Garcia JK, Miltat J (2002) Domain wall dynamics in nanowires. J Magn Magn Mater 242–255:1061–1063

Ueno Y, Horiuchi T, Tate A, Niwa O, Zhou HS, Yamada T, Honma I (2005) Effect of calcination temperature of self-ordered mesoporous silicate on adsorption character of aromatic hydrocarbons. New J Chem 29:504–508

Usov NA, Zhukov A, Gonzalez J (2007) Domain walls and magnetization reversal process in soft magnetic nanowires and nanotubes. J Magn Magn Mater 316:255–261

Von V (2011) Magnetization dynamics in a permalloy disc and nanowire. Konstanzer Online Publikations System (KOPS) URL: http://nbn-resolving.de/urn:nbn:de:bsz:352-182161

Wang YL, Herricks T, Xia YN (2003) Single crystalline nanowires of lead can be synthesized through thermal decomposition of lead acetate in ethylene glycol. Nano Lett 3:1163–1166

Wu KH, Yu CH, Chang YC, Horng DN (2004) Effect of pH on the formation and combustion process of sol–gel auto-combustion derived NiZn ferrite/SiO_2 composites. J Solid State Chem 177:4119–4125

Xu J, Wang H, Fu W, Du K, Sui Y, Chen J, Zeng Y, Li M, Zou G (2007) Preparation and magnetic properties of magnetite nanoparticles by sol–gel method. J Magn Magn Mater 309:307–311

Yang ZH, Li ZW, Kong LB (2010) One-step synthesis of $Ni_{0.23}Cu_{0.11}Zn_{0.66}Fe_2O_4$ ferrite nanowire arrays using a template method. J Alloys Compd 501:173–176

Yu M, Liu J, Li S (2007) Fabrication and characterization of highly ordered Ni0.5Zn0.5Fe2O4 nanowire/tube arrays by sol–gel template method. J Univ Sci Tech Beijing 14:469–472

Zeng H, Skomski R, Menon L, Lin Y, Bandyopadhyay S, Sellmyer DJ (2002) Structure and magnetic properties of ferromagnetic nanowires in self-assembled arrays. Phys Rev B 65:134426134426–134426134428

Zhang D, Tong Z, Xu G, Li S, Ma J (2009) Templated fabrication of $NiFe_2O_4$ nanorods: characterization, magnetic and electrochemical properties. Solid State Sci 11:113–117

Zhao D, Huo Q, Feng J, Chmelka BF, Stucky GD (1998) Nonionic triblock and star diblock copolymer and oligomeric surfactant syntheses of highly ordered, hydrothermally stable, mesoporous silica structures. J Am Chem Soc 120:6024–6036